

# Quantum-to-semiclassical Husimi dynamics of non-Hermitian localization transitions

Pallabi Chatterjee,<sup>1,\*</sup> Bhabani Prasad Mandal,<sup>2,†</sup> and Ranjan Modak<sup>1,‡</sup>

<sup>1</sup>*Indian Institute of Technology Tirupati, Tirupati, India 517619*

<sup>2</sup>*Department of Physics, Banaras Hindu University, Varanasi 221005, India*

The localization transition in the Hermitian Aubry–André model is known to have a clear classical origin, with the critical point being exactly predictable from an analysis of classical phase-space trajectories. Motivated by this correspondence, we investigate whether a similar classical origin exists for localization transitions in non-Hermitian quasiperiodic Hamiltonians. Using semiclassical Husimi dynamics together with a detailed phase-space stability analysis, we show that localization transitions persist even in the semiclassical limit of such non-Hermitian models. However, in sharp contrast to the Hermitian Aubry–André case, the transition point inferred from classical phase-space analysis does not coincide with the quantum critical point. Instead, we find that the semiclassical transition depends sensitively on the choice of the irrational parameter defining the quasiperiodic potential, indicating the absence of a universal classical–quantum correspondence for the localization transition in the non-Hermitian setting. Nonetheless, we identify a suitable parameter regime in which the classical dynamics can faithfully mimic the quantum dynamics over a finite but appreciable time window.

## I. INTRODUCTION

In one-dimensional (1D) non-interacting systems, arbitrarily weak uncorrelated disorder leads to Anderson localization of all single-particle states, resulting in the complete absence of transport[1, 2]. In contrast, quasiperiodic lattice models of non-interacting particles offer a clean and controllable framework for exploring localization phenomena beyond the traditional Anderson paradigm, which can even support localization-delocalization transition in 1D [3]. A quasiperiodic potential can be defined as a deterministic potential characterized by an incommensurability parameter  $\beta$ , such that when  $\beta$  is irrational with respect to the underlying lattice spacing, the potential remains quasiperiodic. With recent experimental advances, particularly in cold atoms and photonic systems, the localization–delocalization transition in these models can now be probed with remarkable precision[4–7]. A wide variety of quasiperiodic potentials have been investigated, revealing rich phase diagrams and diverse localization properties[8–13].

Extending these ideas to open systems [14–17], non-Hermitian Hamiltonians have emerged as a powerful framework for describing non-interacting systems in which energy or particles can exchange with the environment, thus going beyond the conventional Hermitian paradigm. In such non-Hermitian settings, disorder can generate unconventional localization phenomena and metal–insulator transitions. For instance, in a non-Hermitian Anderson-type model with purely imaginary on-site disorder, states can become exponentially localized, showing that non-Hermiticity promotes localization [18]. In contrast, introducing asymmetry in the hopping amplitudes—as in the Hatano–Nelson

model[19]—produces a delocalization transition, illustrating the competition between non-reciprocal transport and disorder. Non-Hermitian extensions of different variants of quasiperiodic models can exhibit even richer behavior. These systems can feature modified localization–delocalization transitions, mobility edges, and entirely new spectral and topological phase transitions that are absent in Hermitian analogs[20–32]. By tuning the complex phase or amplitude of the quasiperiodic potential, it is possible to manipulate the interplay between conventional Anderson localization and the non-Hermitian skin effect[33]. Experimental simulation demonstrated how non-Hermitian effects, combined with disorder, can generate both localization and topologically nontrivial states [34]. In general, non-Hermitian systems have attracted growing interest, motivated by experimental realizations in photonic lattices and ultracold atomic gases [35–39]. A celebrated paradigm in non-Hermitian physics is the parity–time (PT) symmetric class, namely a broad family of non-Hermitian Hamiltonians first introduced by Bender et al., which can exhibit entirely real spectra as long as the PT symmetry is unbroken [40, 41]. PT-symmetric quasiperiodic lattice models have also been realized and have attracted considerable attention [42, 43]. Taken together, these developments establish non-Hermitian quasiperiodic lattices as a powerful platform for investigating unconventional localization phenomena, spectral topology, and the role of openness in quantum systems.

An intriguing question, however, is whether the delocalization–localization transitions observed in quantum quasiperiodic models persist in an analogous classical description. Earlier studies have shown that for the simplest quasiperiodic model—the Aubry–André (AA) model[3]—the quantum critical point can be accurately reproduced from the corresponding classical trajectory [44]. In this work, we extend these ideas to non-Hermitian quasiperiodic systems and investigate whether a classical description can capture such localiza-

\* ph22d001@iittp.ac.in

† bhabani@bhu.ac.in

‡ ranjan@iittp.ac.in

tion–delocalization transitions.

There are several established approaches for treating non-Hermitian systems in phase space. These include formulations based on position and momentum using complexified classical equations of motion with complex phase-space variables [45], as well as descriptions on a real phase space with a modified metric structure, particularly within Gaussian-state dynamics [46]. Related work has derived canonical equations of motion using coherent-state approximations [47], and applied phase-space equations obtained from Gaussian wavepacket approximations to single-band non-Hermitian tight-binding chains [48]. As well as there is study of complexified semiclassical theory [49]. More recently, it has been shown that for non-Hermitian Hamiltonians, a semiclassical approximation leads to an evolution equation for the Husimi distribution [50, 51]. The Husimi distribution is strictly positive and normalizable, thereby providing a well-defined phase-space representation of quantum dynamics [50–56]. For continuous models, the semiclassical Husimi evolution follows canonical phase-space trajectories [57], multiplied by a norm landscape [50], which reduces to unity in Hermitian systems. It has further been established that quantum and classical Husimi flows coincide exactly when the Hamiltonian is bilinear in the creation and annihilation operators, whereas for more general Hamiltonians, the classical Husimi dynamics constitute only a short-time approximation to the full quantum evolution. This motivates us to adopt the Husimi approach and examine whether the time evolution of the semiclassical Husimi function can accurately predict the quantum localization–delocalization transition point in non-Hermitian quasiperiodic systems [58, 59].

Our results show that, in contrast to the Hermitian AA model, the classical Husimi phase-space dynamics of the non-Hermitian model fail to reproduce the correct quantum transition point. This breakdown highlights a fundamental limitation of trajectory-based semiclassical descriptions in non-Hermitian quasiperiodic systems. We further determine the transition point from a fixed-point analysis of the classical trajectory geometry and show that the classical Husimi dynamics follow this geometric transition. Moreover, unlike the Hermitian AA model, the transition point in the non-Hermitian lattice depends explicitly on the incommensurability parameter  $\beta$ , reflecting the irrational quasiperiodicity of the potential. Notably, we identify a special value of  $\beta$  for which the classical and quantum transition points coincide.

The manuscript is organized as follows. In Sec. II, we describe the lattice models, and in Sec. III we discuss the corresponding lattice dynamics. Section IV is devoted to the quantum Husimi dynamics of the continuum models. In Sec. V, we present the semiclassical limit of the models and the associated semiclassical Husimi dynamics. Finally, we conclude in Sec. VI.

## II. MODEL

We analyze two non-Hermitian models, referred to as Model I and Model II. In Model I, Hermiticity is broken through asymmetric hopping, whereas in Model II, non-Hermiticity arises from a complex on-site potential.

### A. Model I

Model I is the non-Hermitian version of the AA model, where the non-Hermiticity has been introduced by the unequal left ( $J_L$ ) and right ( $J_R$ ) hopping terms, and is described by the following Hamiltonian on a lattice of size  $L$ ,

$$H_I = \sum_j (J_L c_j^\dagger c_{j+1} + J_R c_{j+1}^\dagger c_j) + 2V \sum_j \cos(2\pi\beta j) c_j^\dagger c_j, \quad (1)$$

here,  $c_j^\dagger, c_j$  are the creation and annihilation operators respectively, and  $V$  is the strength of the quasiperiodic potential.  $\beta$  is an irrational number. In the Hermitian case, there is a delocalization-localization transition as one tunes the parameter  $V$ , and the transition point is at  $V = J_L = J_R$  [3]. On the other hand, this non-Hermitian model is well studied in [19, 60], where it is found that the transition point of delocalized to localized phase is at  $V_c = J_L$  with  $J_L > J_R$ . In all our calculations, we set  $J_L = 1$  and  $J_R = 1/2$ .

### B. Model II

Another model we study features non-Hermiticity originating from the on-site potential, with the Hamiltonian given by [58],

$$H_{II} = J \sum_j (c_j^\dagger c_{j+1} + c_{j+1}^\dagger c_j) + V \sum_j e^{(-2\pi i \beta j)} c_j^\dagger c_j. \quad (2)$$

Previous numerical results for model II suggest a metal-insulator phase transition at the critical value  $V_c = J$ , which exhibits a PT-symmetric breaking phase transition as well. For  $V_c < J$ , the energy spectrum is entirely real, and all eigenstates are delocalized (metallic and unbroken PT phases), while for  $V_c > J$  the energy spectrum becomes complex and all eigenstates are localized (insulating and PT broken phases). In all our calculations, we set  $J = 1$ . For most of the data presented in this manuscript, we choose  $\beta = (\sqrt{5} - 1)/2$ ; scenarios with different values of  $\beta$  are discussed only in Sec. V.

## III. LATTICE DYNAMICS

Figure 1 shows the dynamical properties of the non-Hermitian lattice models 1 and 2, together with the Hermitian version of Model I, starting from a coherent state.

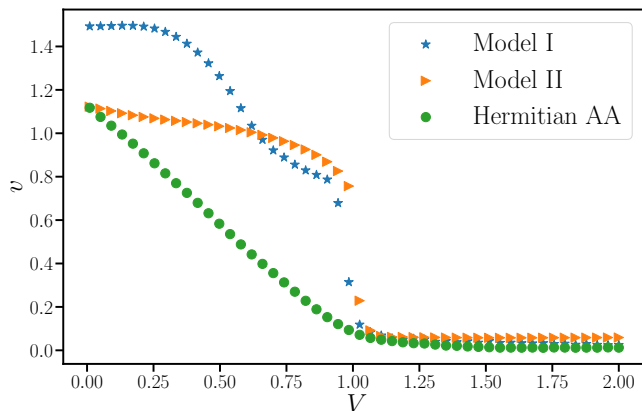


FIG. 1. Velocity of the excitation propagation  $v$  vs.  $V$  at time  $t = 100$ . Results are for Model I, Model II, and the Hermitian AA model. Results are with a starting coherent initial state centred at the centre of the lattice. System size is taken as  $L = 601$ .

We choose as the initial state a minimal-uncertainty (coherent) wave packet centered at the middle of the lattice. Its position-space representation is

$$\psi_j(t=0) = \mathcal{N} \exp\left(-\frac{(j - \frac{L+1}{2})^2}{2}\right)$$

where  $L$  is the system size, taken to be an odd integer, and  $\mathcal{N}$  denotes the normalization constant. In our calculations, we take  $L = 601$ . Starting from this initial state, we calculate the velocity of excitation propagation, defined as

$$v = \lim_{t \rightarrow \infty} \lim_{L \rightarrow \infty} \frac{\sigma(t)}{t}. \quad (3)$$

Here, the wave-packet spread is given by

$$\sigma^2(t) = \frac{\sum_j j^2 |\psi_j(t)|^2}{\sum_j |\psi_j(t)|^2}. \quad (4)$$

The measure  $v$  remains finite as long as the transport is ballistic, i.e., when  $\sigma(t) \propto t$ . In contrast, in the localized phase—and also in the diffusive phase, where  $\sigma(t) \propto t^{1/2}$ —this measure vanishes. For the non-Hermitian model studied here, the transport remains ballistic both in the delocalized phase and at the transition point (see Ref. [59]). Consequently, the measure  $v$  remains finite throughout this regime. In contrast, for the Hermitian version of Model I, the dynamics at the transition point is diffusive (see Ref. [61]), leading to a vanishing value of  $v$ . Therefore, at the transition point,  $v$  is expected to remain finite for the non-Hermitian model, in sharp contrast to its Hermitian model.

In Fig. 1, we present the dependence of the excitation transport velocity  $v$  on the potential strength  $V$ . As  $V$  is increased, the velocity  $v$  decreases and eventually vanishes upon entering the localized phase. While

this behavior is continuous in the Hermitian case with  $J_L = J_R$ , the situation is qualitatively different for the non-Hermitian models. In particular, the transition at the critical point  $V_c = 1$  is discontinuous when characterized in terms of the transport velocity  $v$ , in agreement with previous findings [59]. This discontinuity implies that, even arbitrarily close to the critical point from the delocalized side, the system can sustain a finite ballistic transport velocity, which then drops abruptly to zero as the potential strength is increased beyond  $V_c$ . We also observe that, for certain choices of initial states, the velocity  $v$  initially increases with  $V$ , which is rather counterintuitive and suggests that, in some cases, the strength of the quasiperiodic potential can enhance the speed of excitation transport. For all these calculations, we choose  $\beta = \frac{\sqrt{5}-1}{2}$ , and  $t = 100$  for computing  $v$ . We emphasize that the discontinuity in  $v$  near  $V = 1$  becomes increasingly pronounced with increasing  $t$ , and correspondingly with increasing system size  $L$ .

#### IV. QUANTUM HUSIMI DISTRIBUTION OF THE CONTINUUM MODEL

To gain a phase-space perspective on the underlying quantum dynamics using the Husimi distribution, we first construct the continuum version of the lattice model. The fact that both models considered in this work can be diagonalized in the momentum basis for  $V = 0$  motivates our continuum formulation. Indeed, when  $V = 0$ , both Model I and Model II are translationally invariant, and their Hamiltonians are diagonal in the momentum representation. In this representation, Model I is described by

$$H_I(V=0) = \sum_p (J_R e^{ip} + J_L e^{-ip}) c_p^\dagger c_p, \quad (5)$$

while Model II takes the form

$$H_{II}(V=0) = \sum_p J \cos p c_p^\dagger c_p. \quad (6)$$

Here,  $c_p^\dagger$  and  $c_p$  are creation and annihilation operators in the momentum basis, and we set  $\hbar = 1$ .

Hence, we write the continuous version of Model I as,

$$H_I^q = J_R e^{i\hat{p}} + J_L e^{-i\hat{p}} + 2V \cos(2\pi\beta\hat{q}), \quad (7)$$

with,  $\hat{p} = \frac{i(\hat{a}^\dagger - \hat{a})}{\sqrt{2}}$  and  $\hat{q} = \frac{(\hat{a}^\dagger + \hat{a})}{\sqrt{2}}$ , where  $a, a^\dagger$  are the Harmonic oscillator's (bosonic) creation and annihilation operators.

Similarly, for Model II, we write the continuous model as,

$$H_{II}^q = 2J \cos \hat{p} + V e^{(-2i\pi\beta\hat{q})}. \quad (8)$$

An analogous strategy has also been employed in earlier studies in different contexts [62].

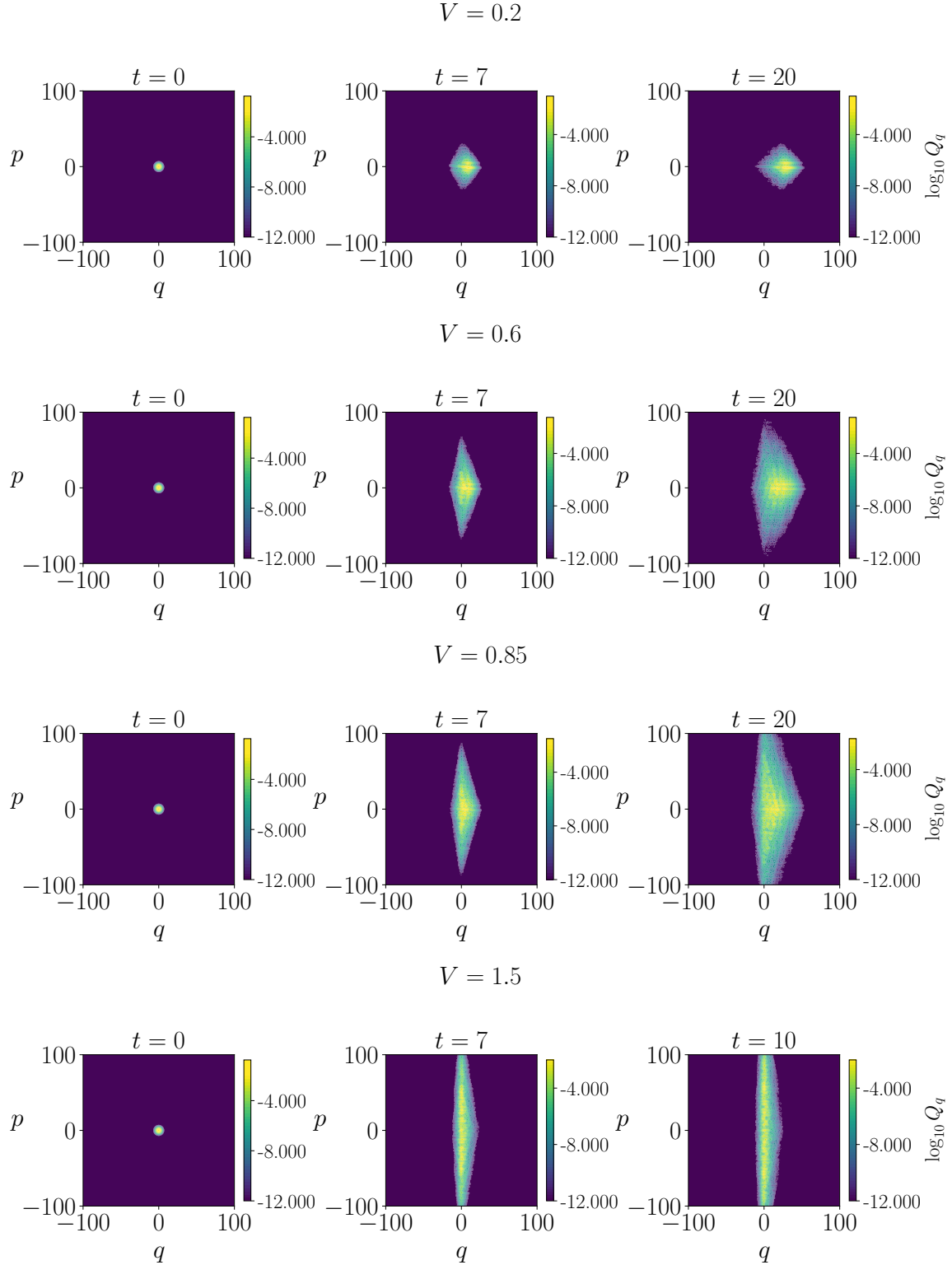


FIG. 2. Quantum Husimi distribution at different time instances starting from coherent state  $|0\rangle$  and evolving under the Hamiltonian [Eq. (7)] continuous version of the Model I. Data is for  $V = 0.2, 0.6, 0.85, 1.5$ . The color code represents the Husimi values.

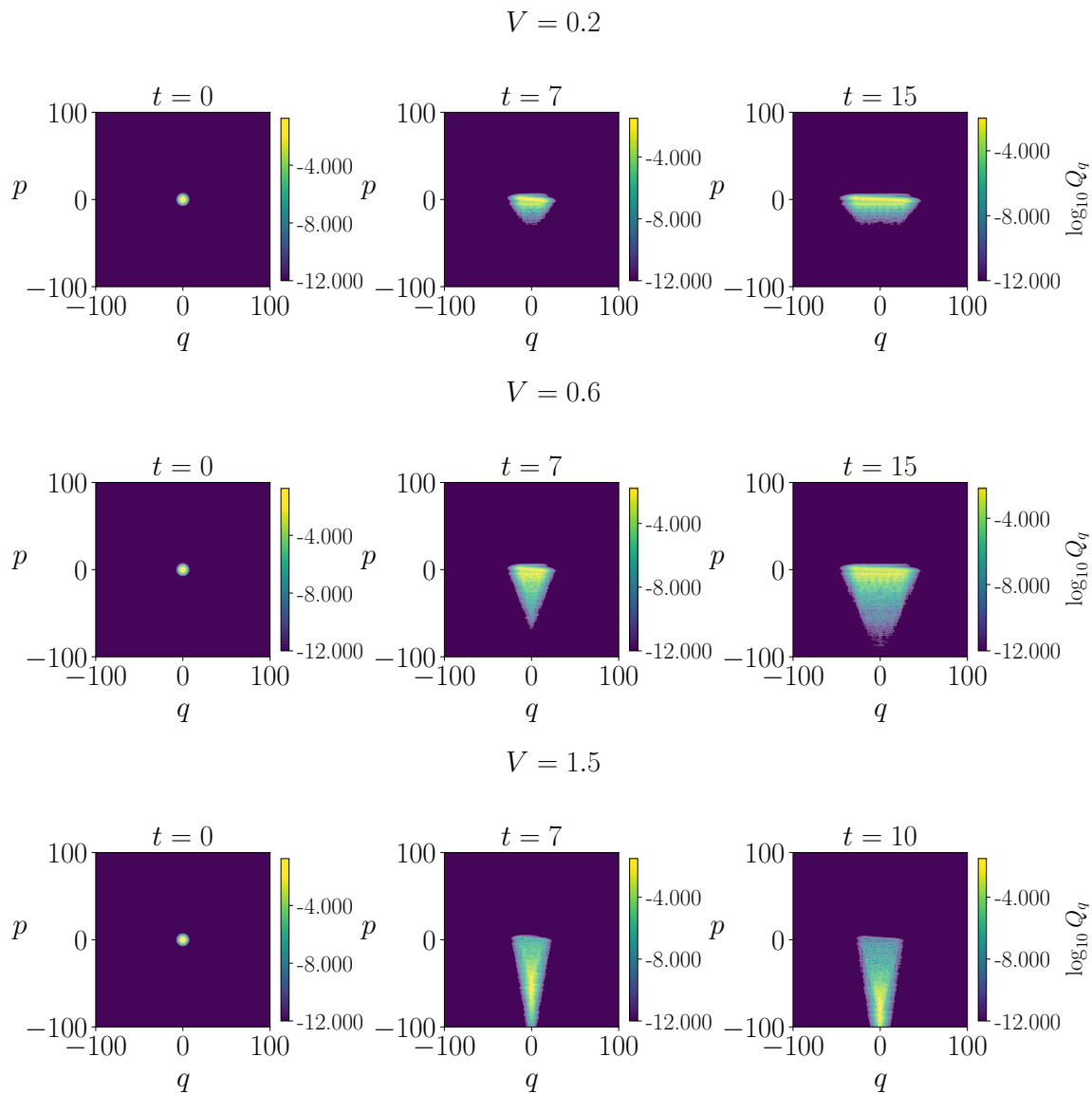


FIG. 3. Quantum Husimi distribution at different time instances starting from coherent state  $|0\rangle$  and evolving under the Hamiltonian [ Eq. (8)] continuous version of the Model II. Data is for  $V = 0.2, 0.6, 1.5$ . The color code represents the Husimi values.

Husimi distribution, which is a phase-space representation of the quantum state  $|\psi(t)\rangle$ , is given by [50, 51].

$$Q_q(t) = |\langle z|\psi(t)\rangle|^2, \quad (9)$$

where  $|z\rangle = \hat{D}(z)|0\rangle = e^{za^\dagger - z^*a}|0\rangle$ , where  $|0\rangle$  is the ground state of Harmonic oscillator and  $z = (q + ip)/\sqrt{2}$  ( $q$  and  $p$  are eigenvalues of the position  $\hat{q}$  and momentum  $\hat{p}$  operators), hence  $|z\rangle$  is a coherent state displaced by the displacement operator  $\hat{D}$ . We start from an initial coherent state  $|0\rangle$  and evolve it under the non-Hermitian Hamiltonian  $H_{\text{NH}}$  (which, in our case, corresponds to Eqs. (7) and (8)). The time-evolved state is given by

$|\psi(t)\rangle = \frac{e^{-itH_{\text{NH}}}|0\rangle}{\|e^{-itH_{\text{NH}}}|0\rangle\|}$ . We then compute the overlap of this state with displaced coherent states at different points in phase space. The squared modulus of this overlap yields the quantum Husimi distribution at different time instants. To quantify the spreading of the Husimi distribution with time, we also calculate the variance of the Husimi distribution as,

$$\sigma_H^2 = \frac{\int q^2 Q_q(q, p, t) dp dq}{\int Q_q(q, p, t) dp dq}. \quad (10)$$

*Model I:* In Fig. 2, we show the time evolution of the Husimi distribution at different time instants for  $V = 0.2, 0.6, 0.85, \text{ and } 1.5$  for the continuous version of Model I

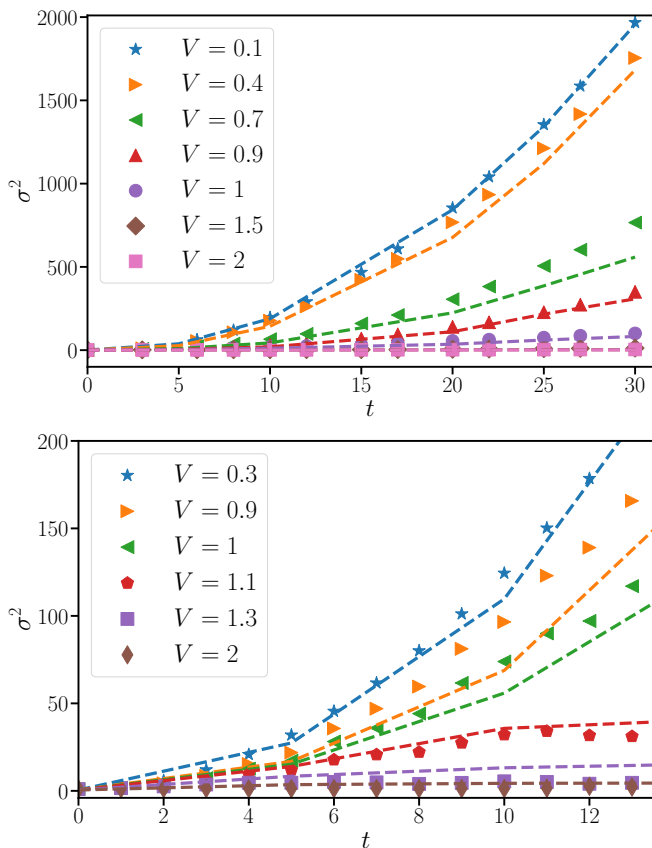


FIG. 4. Upper panel: Comparison of  $\sigma^2$  vs.  $t$  plots for non-Hermitian quantum continuous Model I [Eq. (7)] and its corresponding lattice model, for  $\beta = \frac{\sqrt{5}-1}{2}$ . The symbols represent the quantum continuous model, and dashed lines represent the data for its lattice version. The lower panel represents the same for Model II(8) and its lattice version.

[Eq. (7)]. We observe that up to  $V = 1$  the distribution continues to spread along the  $q$  direction, whereas for  $V > 1$  the spreading in the  $q$  direction is suppressed. As is well known, wave-function propagation in the corresponding non-Hermitian lattice model is unidirectional, with the direction determined by the larger of  $J_L$  and  $J_R$  [19]. The continuous quantum model faithfully reproduces this behavior and correctly captures the transition point at  $V_c = J_L$ .

We also present the time dependence of the variance of the Husimi distribution in the upper panel of Fig. 4. In the small- $V$  limit, we observe  $\sigma^2(t) \sim t^2$ , indicating ballistic spreading. As  $V$  is increased, the ballistic spreading gradually slows down, and for  $V > 1$  the variance essentially saturates, approaching  $\sigma^2 \sim t^0$ . This behavior signals a delocalization–localization transition at  $V_c = J_L$  for Model I. In our numerically accessible parameter regime, we simulate the dynamics up to time  $t = 30$ . In the quantum continuum model, accurate long-time evolution demands a large matrix dimension to control numerical errors. Additionally, the presence of Gaussian functions in position space, which decay expo-

entially fast for large  $x$ , poses significant challenges in maintaining numerical precision. We also compare these results with the corresponding lattice calculations: the symbols represent data from the continuous model, while dashed lines denote the lattice dynamics. Strictly speaking, Eq. (4) and Eq. (10) correspond to different quantities; therefore, their numerical values need not coincide. However, the qualitative time dependence of  $\sigma^2(t)$  is similar in both cases.

*Model II* Similar to the previous model, we observe the time evolution of the quantum Husimi distribution for Model II [Eq. (8)] in Fig. 3 for different values of  $V$ . The spreading of the distribution in phase space correctly identifies the phase transition point at  $V_c = J$ : for  $V < V_c$  the distribution spreads along the  $q$  direction, while for  $V > V_c$  the spreading in the  $q$  direction is suppressed.

We present the time dependence of the variance of the Husimi distribution in the lower panel of Fig. 4. We observe that  $\sigma^2(t) \sim t^2$  for  $V < V_c = J = 1$ , while it ceases to increase with time once  $V > V_c$ . This behavior indicates a delocalization–localization transition at  $V_c = J = 1$ . We also compare these results with those obtained from the corresponding lattice models and find reasonable agreement between the two.

In hindsight, these results confirm that the continuum version of our non-Hermitian lattice model provides a reasonable approximation and efficiently reproduces the phase transition observed in the lattice models within the same parameter regime.

## V. SEMICLASSICAL LIMIT OF THE HUSIMI DISTRIBUTION

In this section, we analyze the semiclassical limit of the quantum Husimi dynamics presented in the previous section. Our aim is to investigate whether the semiclassical description can capture and predict the localization–delocalization transition in the non-Hermitian Model I and Model II.

### A. Formalism

First, for the sake of completeness, we briefly outline the formalism required to take the appropriate semiclassical limit of the quantum Husimi dynamics, which has already been discussed in detail in Refs. [50, 51]. The time evolution of the quantum Husimi function  $Q_q$  (which was defined in Eq. (9)) under any non-Hermitian Hamiltonian  $H_{\text{NH}}$  could be written as,

$$i \frac{\partial Q_q}{\partial t} = \langle z | H_{\text{NH}} | \psi \rangle \langle \psi | z \rangle - \langle z | \psi \rangle \langle \psi | H_{\text{NH}}^\dagger | z \rangle.$$

Considering  $H_{\text{NH}}$  is an analytic function of creation and annihilation operators, in normal order form, we can ex-

pand any general non-Hermitian Hamiltonian as,

$$H_{\text{NH}} = \sum_{m,n=0}^{\infty} K_{m,n} a^{\dagger m} a^n,$$

where  $K_{m,n}$  are complex coefficients. Then the evolution becomes,

$$i \frac{\partial Q_q}{\partial t} = \sum_{m,n} K_{m,n} z^{*m} \langle z | a^n | \psi \rangle \langle \psi | z \rangle - K_{m,n}^* z^* \langle z | \psi \rangle \langle \psi | a^{\dagger n} | z \rangle.$$

One can use,

$$a^n |z\rangle = z^n |z\rangle, \\ \langle z | \psi \rangle \langle \psi | a^{\dagger n} | z \rangle = e^{-|z|^2} \frac{\partial^n}{\partial z^n} [Q_q(z) e^{|z|^2}].$$

It is clear that, upon substituting these coherent-state identities, one obtains a higher-order differential equation for the Husimi distribution. If we neglect all higher-order derivatives beyond the first-order terms, the resulting equation for the evolution of the Husimi distribution reads as,

$$\frac{\partial Q_{cl}}{\partial t} + i \frac{\partial H^c}{\partial z} \frac{\partial Q_{cl}}{\partial z^*} - i \frac{\partial H^{c*}}{\partial z^*} \frac{\partial Q_{cl}}{\partial z} - 2\Gamma_I Q_{cl} = 0, \quad (11)$$

which we refer to as the semiclassical evolution equation for the Husimi dynamics. In Eq. (11), we denote the Husimi distribution by  $Q_{cl}$  instead of  $Q_q$  to emphasize that the solution of this equation represents the semiclassical approximation to the full quantum Husimi distribution  $Q_q$ . Here  $H^c$  is the classical counterpart of the non-Hermitian Hamiltonian, and can be written as,

$$H^c = \sum_{m,n=0}^{\infty} K_{m,n} z^{*m} z^n,$$

and the imaginary part of  $H^c$  is identified as  $\Gamma_I = \frac{1}{2i}(H^c - H^{c*})$ , and the real part as  $\Gamma_R = \frac{1}{2}(H^c + H^{c*})$ . The semiclassical Husimi dynamics equation Eq. (11) can be solved using the method of characteristics, and one can find the solution as,

$$Q_{cl}(z, t) = Q_{cl}^0(\zeta_0(z, t)) w(z, t). \quad (12)$$

This suggests starting from a given initial Husimi function  $Q_{cl}^0(z, t=0)$ , to calculate the time evolution of the Husimi distribution, we need to evolve it backward along a trajectory given by,

$$\dot{\zeta} = -i \frac{\partial H^{c*}}{\partial \zeta^*}. \quad (13)$$

$\zeta_0(z, t)$  represents the initial condition of the above trajectory such that  $\zeta(t) = z$ . Then we need to multiply this by the norm factor, which evolves as,

$$\dot{w}(z, t) = 2\Gamma_I(\zeta_0(z, t)) w(z, t),$$

with initial condition  $w(z, 0) = 1$ . We note that the semiclassical solution of the Husimi distribution coincides exactly with the full quantum Husimi distribution only for Hamiltonians that are quadratic in the creation and annihilation operators  $a^{\dagger}$  and  $a$ . This condition is not satisfied for either Model I or Model II. Consequently, we do not expect exact quantitative agreement between the semiclassical and quantum Husimi dynamics. Nevertheless, our aim is to examine whether the semiclassical description can still capture the essential physics underlying the localization-delocalization transition in these models.

## B. Trajectory analysis

Since the semiclassical time evolution of the Husimi distribution is governed by the underlying phase-space trajectories [Eq. (13)], we perform a detailed analysis of these trajectories using fixed-point analysis. In this context, we like to point out that, in another approach [57], canonical equations of motion were derived for a generic non-Hermitian Hamiltonian within a coherent-state approximation. These equations closely correspond to the trajectory equations employed in our semiclassical Husimi dynamics, up to a reversal of the time direction. We have verified that analyzing the trajectories using either formulation leads to the same geometric transition at the level of phase-space dynamics.

### 1. Trajectory analysis of Model I

First, we replace the operator  $\hat{p}$  and  $\hat{q}$  with dynamical variables  $p$  and  $q$  in Eq. (7), and identified the classical version of the model I as [47, 63],

$$H_I^c = J_R e^{ip} + J_L e^{-ip} + 2V \cos(2\pi\beta q). \quad (14)$$

and the trajectory equation Eq. (13) in terms of  $q, p$  can be written as,

$$\dot{q} = -\frac{\partial \Gamma_R}{\partial p} + \frac{\partial \Gamma_I}{\partial q} = f(q, p) \\ \dot{p} = \frac{\partial \Gamma_R}{\partial q} + \frac{\partial \Gamma_I}{\partial p} = g(q, p), \quad (15)$$

where,  $f(q, p) = (J_R + J_L) \sin p$  and  $g(q, p) = (J_R - J_L) \cos p - 4\pi\beta V \sin(2\pi\beta q)$ . Here,  $\Gamma_R$  refers to the real part of the Hamiltonian  $H_I^c$ , and  $\Gamma_I$  is the imaginary part of the Hamiltonian  $H_I^c$ .

Next, our goal is to investigate the phase-space portrait of the dynamical system described by Eq. (15). Moreover, we examine whether there exists a critical value  $V_c$  such that  $V \geq V_c$  the trajectories remain bounded in the  $q$  direction, which would imply that the dynamics is localized in position space. Note that, in the quantum models (both lattice and continuum), there exists such a critical value  $V = V_c$  that separates the delocalized and localized phases. Although the dynamical equations can be solved

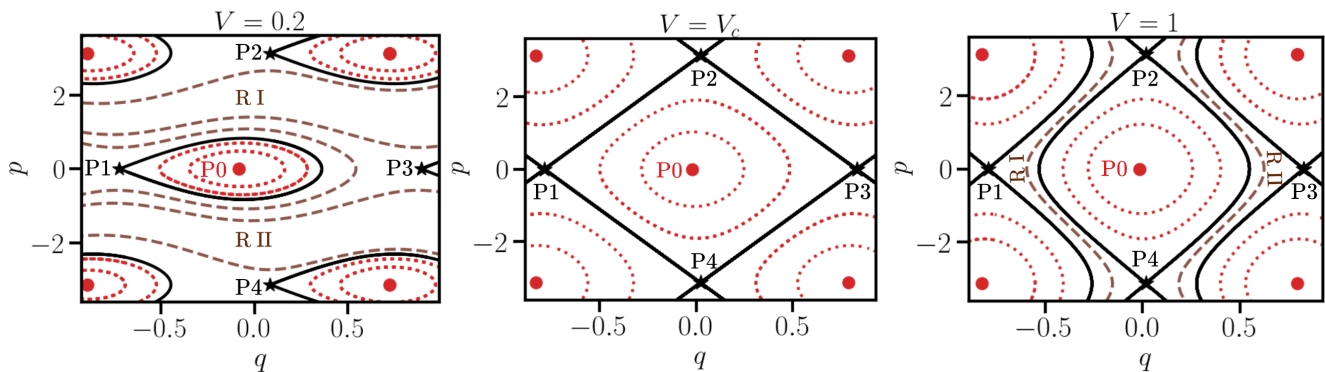


FIG. 5. Trajectory evolution governed by the semiclassical Hamiltonian of Model I [Eq. (14)] at different  $V$  values. Trajectory evolution shows a transition near  $V_c = \frac{1}{2}\sqrt{(J_L + J_R)^2 + \frac{4\Delta^2}{(4\pi\beta)^2}} \sim 0.752$ . Data are for  $J_L = 1, J_R = 0.5$ .  $\beta = \frac{\sqrt{5}-1}{2}$ .

numerically and the phase portrait can be analyzed to identify the critical value  $V_c$ , it is in general, difficult to pinpoint  $V_c$  accurately from numerical simulations alone. We therefore adopt the following strategy: we first determine the fixed points of the dynamical system and analyze the dynamics in their vicinity by linearizing the equations of motion. This allows us to obtain an analytical estimate of  $V_c$ , which we then compare with the numerical results.

We find the fixed points of the Eq. (15), and they are,

$$\begin{aligned} \dot{q} = 0 & \text{ gives } p_0 = n\pi, n = 0, \pm 1, \pm 2 \dots \\ \dot{p} = 0 & \text{ gives } q_0 = \frac{1}{2\pi\beta} \sin^{-1} \frac{\Delta(-1)^n}{4\pi\beta V}. \end{aligned}$$

Note that the fixed point solutions exist only if the following conditions are satisfied,

$$|\Delta| \leq 4\pi\beta V; \quad \Delta = J_R - J_L.$$

We have verified numerically that solutions of Eq. (15) remain unbounded in the  $q$  direction for  $|\Delta| > 4\pi\beta V$ .

Linearization of the equations of motion  $\dot{q} = f(q, p)$  and  $\dot{p} = g(q, p)$  about a fixed point  $(q_0, p_0)$  yields the equations governing small fluctuations around the fixed point. Defining  $\delta q = q - q_0$  and  $\delta p = p - p_0$ , the corresponding linearized equations of motion can be written as,

$$\begin{pmatrix} \dot{\delta q} \\ \dot{\delta p} \end{pmatrix} = \begin{pmatrix} \frac{\delta f}{\delta q} & \frac{\delta f}{\delta p} \\ \frac{\delta g}{\delta q} & \frac{\delta g}{\delta p} \end{pmatrix}_{(q_0, p_0)} \begin{pmatrix} \delta q \\ \delta p \end{pmatrix} = J \begin{pmatrix} \delta q \\ \delta p \end{pmatrix}. \quad (16)$$

The stability of a fixed point is determined by the nature of the eigenvalues  $\lambda$  of the Jacobian matrix  $J$ . These eigenvalues are obtained from the characteristic equation,

$$\lambda^2 = -2(2\pi\beta)^2 V (J_L + J_R) \cos p_0 \cos(2\pi\beta q_0), \quad (17)$$

Now, for  $p_0 = 0$  along with  $\cos(2\pi\beta q_0) = \sqrt{1 - \frac{\Delta^2}{(4\pi\beta V)^2}}$ , and  $p_0 = \pi$  along with  $\cos(2\pi\beta q_0) = -\sqrt{1 - \frac{\Delta^2}{(4\pi\beta V)^2}}$ ,

the fixed points are stable, as the corresponding eigenvalues are purely imaginary. In contrast, for  $p_0 = 0$  along with  $\cos(2\pi\beta q_0) = -\sqrt{1 - \frac{\Delta^2}{(4\pi\beta V)^2}}$ , and  $p_0 = \pi$  along with  $\cos(2\pi\beta q_0) = \sqrt{1 - \frac{\Delta^2}{(4\pi\beta V)^2}}$ , the fixed points are saddle points, characterized by one positive and one negative real eigenvalue. Figure 5 clearly demonstrates this behavior. For example, when  $V = 0.2$ , the stable fixed points are indicated by red dots, while the saddle points are marked by black stars. Trajectories that pass through the saddle points define the separatrix (shown as the solid black curve), which separates the bounded from unbounded trajectories. In the neighborhood of the stable fixed point, the trajectories are closed (identified as red dotted lines in the figures). In contrast, in regions RI and RII (see Fig. 5), the orbits are unbounded in the  $q$  direction, implying delocalization in the spatial dimension. Therefore, in order to identify a critical value  $V_c$  such that delocalization in the spatial direction is absent, regions RI and RII must shrink and eventually disappear. This can only occur if there exist separatrix trajectories that connect the two saddle points. Once  $V > V_c$ , one expects the separatrix to align in such a way that it separates bounded closed orbits governed by the stable fixed point from unbounded orbits in the  $p$  direction, which has been observed for  $V = 1$  (see Fig. 5).

The essential goal is to determine the critical value  $V = V_c$  such that the separatrix trajectory passes through the two saddle points (denoted as points P1 and P2 in Fig. 5). Although we focus on the P1 and P2 points, the symmetry of the phase portrait makes it straightforward to extend the same argument to separatrices passing through the P1 and P4 or the P3 and P4 points.

One can combine the dynamical Eq. (15) to obtain  $dp/dq = g(q, p)/f(q, p)$ . In general, this equation is too complicated to solve analytically for arbitrary  $V$ . Therefore, we expand the trajectory  $p(q)$  to second order in  $q$  in the neighborhood of a saddle point, say P1 (which we refer to  $(q_0, p_0)$  point in the phase portrait) as,

$$p(q) = p_0 + m_1(q - q_0) + \frac{m_2}{2}(q - q_0)^2.$$

By matching coefficients order by order in  $(q - q_0)$ , we obtain explicit expressions for  $m_1$  and  $m_2$  as a function of  $V$ ,

$$m_1 = \pm \frac{-2(2\pi\beta)^2 \cos(2\pi\beta q_0)V}{(J_R + J_L) \cos p_0},$$

$$m_2 = \frac{2}{3m_1} \left[ \frac{(2\pi\beta)^3 \sin(2\pi\beta q_0 V) - \frac{1}{2}m_1^2(J_R - J_L) \cos p_0}{(J_R + J_L) \cos p_0} \right].$$

It is reasonably straightforward to see that the coefficient  $m_2$  changes sign at some value  $V = V_* = \frac{1}{2}\sqrt{(J_L + J_R)^2 + \frac{4\Delta^2}{(4\pi\beta)^2}}$  and  $m_2$  is zero at this choice of  $V$ .

Combining this observation with the behavior of numerically simulated phase trajectories, we are led to conjecture that  $V = V_*$  plays a special role. In particular, near this value of  $V$ , the curvature of the phase trajectories changes sign, which intuitively suggests a transition in the nature of the unbounded regions of the phase portrait—from unbounded motion in the  $q$  direction to unbounded motion in the  $p$  direction, or vice versa. This observation motivates us to compute the slope  $m_1$  at  $V = V_*$ . We find that  $m_1$  at  $V = V_*$  exactly coincides with the slope of the straight line connecting the fixed points P1 and P2 (or equivalently, P1 and P3). Based on this, we first conjecture and then explicitly demonstrate that

$$p = p_0 + m_1(q - q_0)$$

is an exact solution of the differential equation  $dp/dq = g(q, p)/f(q, p)$  at  $V = V_*$ . This implies that, for  $V = V_*$ , the line  $p = p_0 + m_1(q - q_0)$  represents the separatrix trajectory passing through both P1 and P2. Hence, it proves that the critical value of the localization transition  $V_c = V_*$ .

Note that the dynamical equations in Eq. (15) are not Hamiltonian equations in the conventional sense. For a usual time-independent Hamiltonian system, each curve in the phase portrait corresponds to a constant energy contour. Consequently, the shrinking of regions RI and RII can be identified by equating the energies of the saddle points, which automatically implies the existence of a separatrix passing through both saddles [44, 64]. We employ a similar strategy to determine the transition point for the Hermitian Aubry–André model in the Appendix. A.

Applying the same approach to the present case is, however, nontrivial, since the underlying dynamical equations are non-Hamiltonian in nature. Interestingly, we find that the imaginary part of the complex Hamiltonian vanishes at the saddle fixed points. This observation allows us to equate the real parts of the energies at the two saddle points, which correctly reproduces the transi-

tion point obtained earlier, i.e.,

$$-(J_L + J_R) + 2V_c \sqrt{1 - \frac{\Delta^2}{(4\pi\beta V_c)^2}} = (J_L + J_R)$$

$$-2V_c \sqrt{1 - \frac{\Delta^2}{(4\pi\beta V_c)^2}},$$

which yields

$$V_c = \frac{1}{2} \sqrt{(J_L + J_R)^2 + \frac{4\Delta^2}{(4\pi\beta)^2}}.$$

We make two interesting observations: (i) the unbounded orbits in the  $q$  direction are also unidirectional (see Region RI and RII in Fig 5 for  $V = 0.2$ ), which is a signature of the asymmetric hopping terms in the underlying quantum model; (ii) Unlike the Hermitian Aubry–André model (see Appendix. A), the classical transition point in the present case is  $\beta$  dependent. We identify a special value of  $\beta$  for which the classical and quantum transition points coincide, given by,

$$\beta = \frac{1}{2\pi\sqrt{7}}; \quad \text{with} \quad J_R = \frac{J_L}{2}, \quad J_L = 1.$$

We discuss  $\beta = \frac{1}{2\pi\sqrt{7}}$  separately later.

## 2. Trajectory analysis of Model II

The semiclassical version of Model II can be obtained by replacing the operators  $\hat{q}$  and  $\hat{p}$  in Eq. (8) with the corresponding classical variables  $q$  and  $p$ , respectively.

$$H_{II}^c = 2 \cos p + V e^{-2\pi i \beta q}. \quad (18)$$

We take  $J = 1$ . The trajectory equation (Eq. (13)) reads as,

$$\dot{q} = 2 \sin p - 2\pi\beta V \cos(2\pi\beta q)$$

$$\dot{p} = -2\pi\beta V \sin(2\pi\beta q).$$

We follow the same strategy as before and identify the fixed points for  $\pi\beta V \leq 1$  as,

$$\dot{p} = 0 \quad \text{gives} \quad q_0 = n\pi/(2\pi\beta), \quad n = 0, \pm 1, \pm 2 \dots,$$

$$\dot{q} = 0 \quad \text{gives} \quad p_0 = \sin^{-1}[\pi\beta V(-1)^n].$$

The eigenvalues of the Jacobian matrix  $J$  are given by the following equation,

$$\lambda^2 = -2(2\pi\beta)^2 V \cos p_0 \cos(2\pi\beta q_0).$$

For the combinations  $q_0 = 0, \cos(p_0) = \sqrt{1 - (\pi\beta V)^2}$  and  $q_0 = \pi/(2\pi\beta), \cos(p_0) = -\sqrt{1 - (\pi\beta V)^2}$  we have stable fixed points as the roots are completely imaginary, on the other hand for,  $q_0 = 0, \cos(p_0) = -\sqrt{1 - (\pi\beta V)^2}$

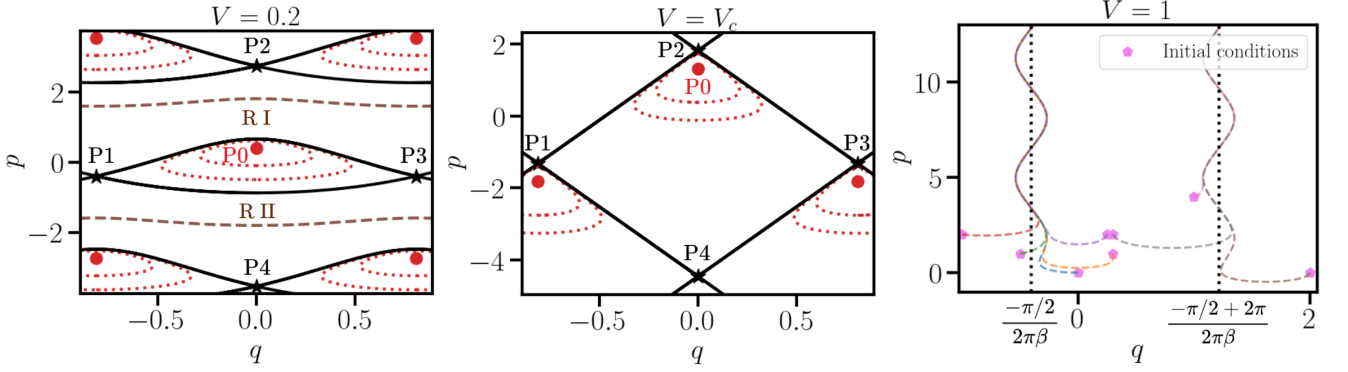


FIG. 6. Trajectory evolution governed by the semiclassical Hamiltonian of Model II [Eq. (18)] at different  $V$  values. Trajectory evolution shows a transition near  $V_c = \frac{2}{\sqrt{1+(2\pi\beta)^2}} \sim 0.498$ . Data are for  $J = 1$ .  $\beta = \frac{\sqrt{5}-1}{2}$ .

and  $q_0 = \pi/(2\pi\beta)$ ,  $\cos(p_0) = \sqrt{1 - (\pi\beta V)^2}$  we have saddle fixed points as we have one positive real and another negative real eigenvalue.

Next, we again perform a rigorous analysis, following the same procedure as before, and analytically determine the transition point as

$$V_c = \frac{2}{\sqrt{1 + (2\pi\beta)^2}},$$

which is also  $\beta$  dependent. In Fig. 6, we present the trajectory evolution for  $\beta = \frac{\sqrt{5}-1}{2}$ . The geometrical changes visible in the trajectories signal a transition, which agrees well with the analytically predicted transition point obtained from the saddle-point analysis. Once again, we find a special value of  $\beta = \frac{\sqrt{3}}{2\pi}$  for which the transition point is  $V_c = 1$ , in agreement with the corresponding quantum transition point.

The large- $V$  ( $V \gg V_c$ ) behavior can also be understood analytically. In the potential-dominated limit  $V \rightarrow \infty$ , the equations of motion reduce to

$$\begin{aligned} \dot{q} &\simeq -2\pi\beta V \cos(2\pi\beta q), \\ \dot{p} &\simeq -2\pi\beta V \sin(2\pi\beta q). \end{aligned}$$

Since  $\dot{q}$  depends only on  $q$ , the first equation can be solved straightforwardly, yielding

$$|\sec(2\pi\beta q(t)) + \tan(2\pi\beta q(t))| = A e^{-(2\pi\beta)^2 V t},$$

where  $A$  is an integration constant determined by the initial condition  $(q_0, p_0)$ . For sufficiently large  $V$  and long times  $t$ , the right-hand side vanishes exponentially, and we obtain

$$|\sec(2\pi\beta q(t)) + \tan(2\pi\beta q(t))| \simeq 0.$$

This implies

$$1 + \sin(2\pi\beta q(t)) = 0,$$

so that

$$q(t) = \frac{-\pi/2 + 2n\pi}{2\pi\beta}, \quad n = 0, \pm 1, \pm 2, \dots$$

Thus, for sufficiently large  $V$  and long times,  $q(t)$  becomes pinned to these discrete values, irrespective of the initial condition. Substituting  $q(t) = \frac{-\pi/2 + 2n\pi}{2\pi\beta}$  into the equation for  $\dot{p}$ , we obtain

$$p(t) = p_0 + 2\pi\beta V t,$$

indicating unbounded linear growth in the  $p$  direction. In the rightmost panel of Fig. 6, this behavior is already visible even for  $V = 1$ . At long times,  $q(t)$  approaches the quantized values given above, while  $p(t)$  exhibits unbounded motion, oscillating around these pinned values of  $q(t)$ . The quantized values of  $q(t)$  are indicated by black dotted lines.

### C. Time evolution of the semiclassical Husimi distribution

Next, we study the time evolution of the semiclassical Husimi distribution governed by Eq. (12) for different values of  $V$  at various time instances, for both Model I and Model II. We choose an initial coherent state  $|z_0\rangle = |0\rangle$ , such that the initial Husimi distribution is given by

$$Q_{\text{cl}}^0(z, t = 0) = e^{-|z|^2}. \quad (19)$$

#### 1. Semiclassical Husimi dynamics of Model I

In Fig. 7, we show the time evolution of the semiclassical Husimi distribution for Model I at  $V = 0.2, 0.752$ , and  $1$ , respectively. As expected, the Husimi dynamics follows the underlying classical trajectories, modulated by the corresponding norm factor. From our earlier analysis

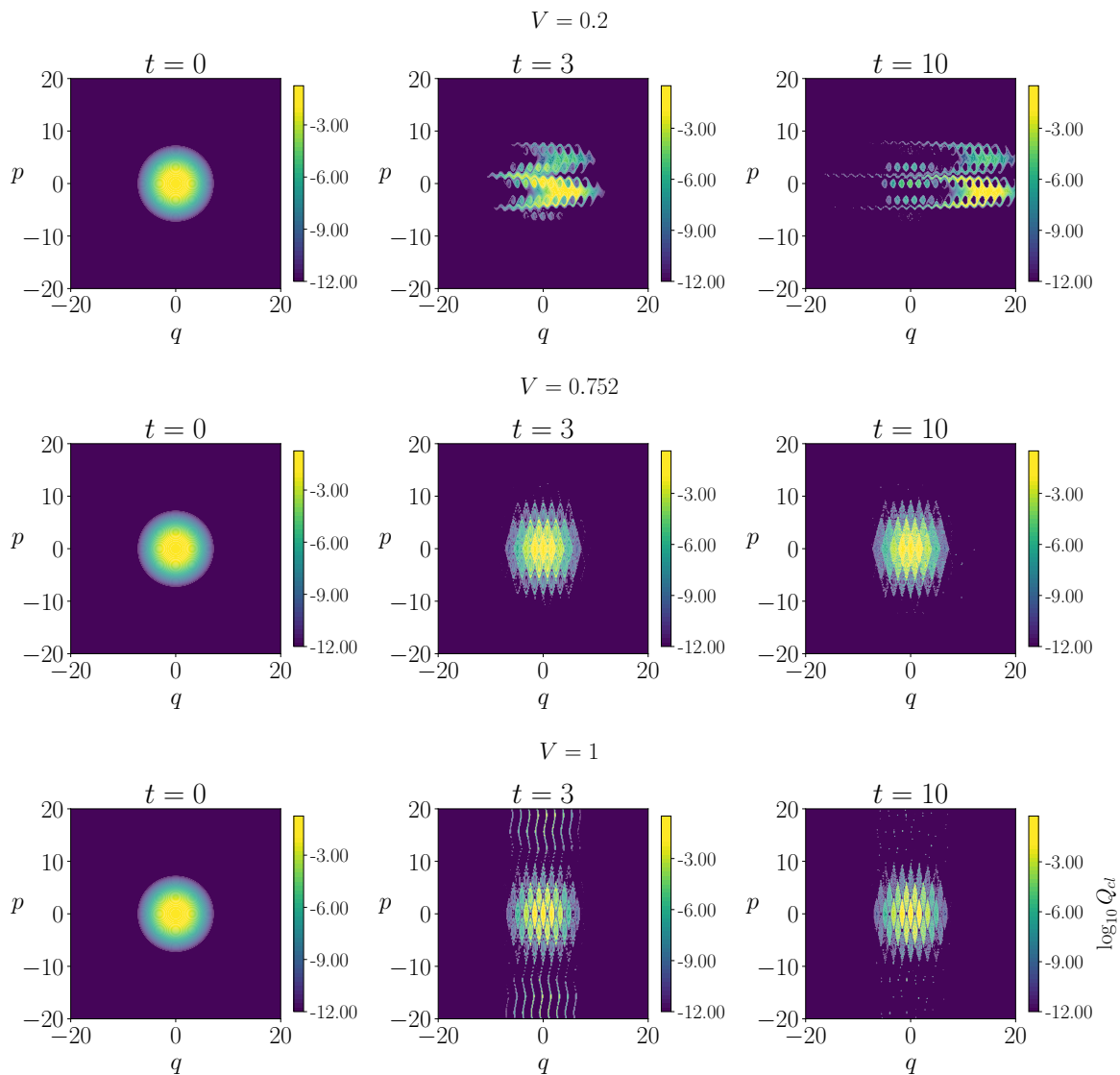


FIG. 7. Semiclassical Husimi distribution at different time instances starting from coherent state  $|0\rangle$  and evolving under the Hamiltonian [Eq. (14)]. Data is for  $V = 0.2, 0.752, 1$ . The color code represents the Husimi values.

of the classical trajectory dynamics, we know that a transition occurs at  $V_c \simeq 0.752$  for  $\beta = (\sqrt{5} - 1)/2$ ,  $J_L = 1$ , and  $J_R = 0.5$ . Consistently, the semiclassical Husimi dynamics also signals a transition near  $V \simeq 0.752$ , as evidenced by the cessation of spreading of the distribution along the  $q$ -direction. We have verified that this conclusion remains unchanged even when the initial state is not chosen to be a coherent state.

Further, we compare the dynamical properties of the lattice model—quantified previously via the speed of propagation—with those obtained from the time evolution of the Husimi distribution of the corresponding continuous quantum model, as well as from the semiclassical Husimi dynamics. As discussed earlier and shown in the upper panel of Fig. 9, for  $\beta = (\sqrt{5} - 1)/2$  and at the fixed time instant  $t = 30$ , the continuous model exhibits dynamical behavior very similar to that of its

lattice counterpart, with both showing a transition near  $V \simeq 1$ . In contrast, the speed of propagation extracted from the semiclassical Husimi distribution drops already near  $V_c \sim 0.752$ , coinciding with the merging of separatrices in the classical phase space. In summary, both the semiclassical Husimi dynamics and the classical trajectory analysis systematically underestimate the quantum localization transition point.

## 2. Semiclassical Husimi dynamics of Model II

A similar analysis is carried out for Model II, leading to the same qualitative conclusions, as shown in Fig. 8. In this case, the transition point extracted from the semiclassical Husimi dynamics closely follows the transition predicted by the classical trajectory analysis,

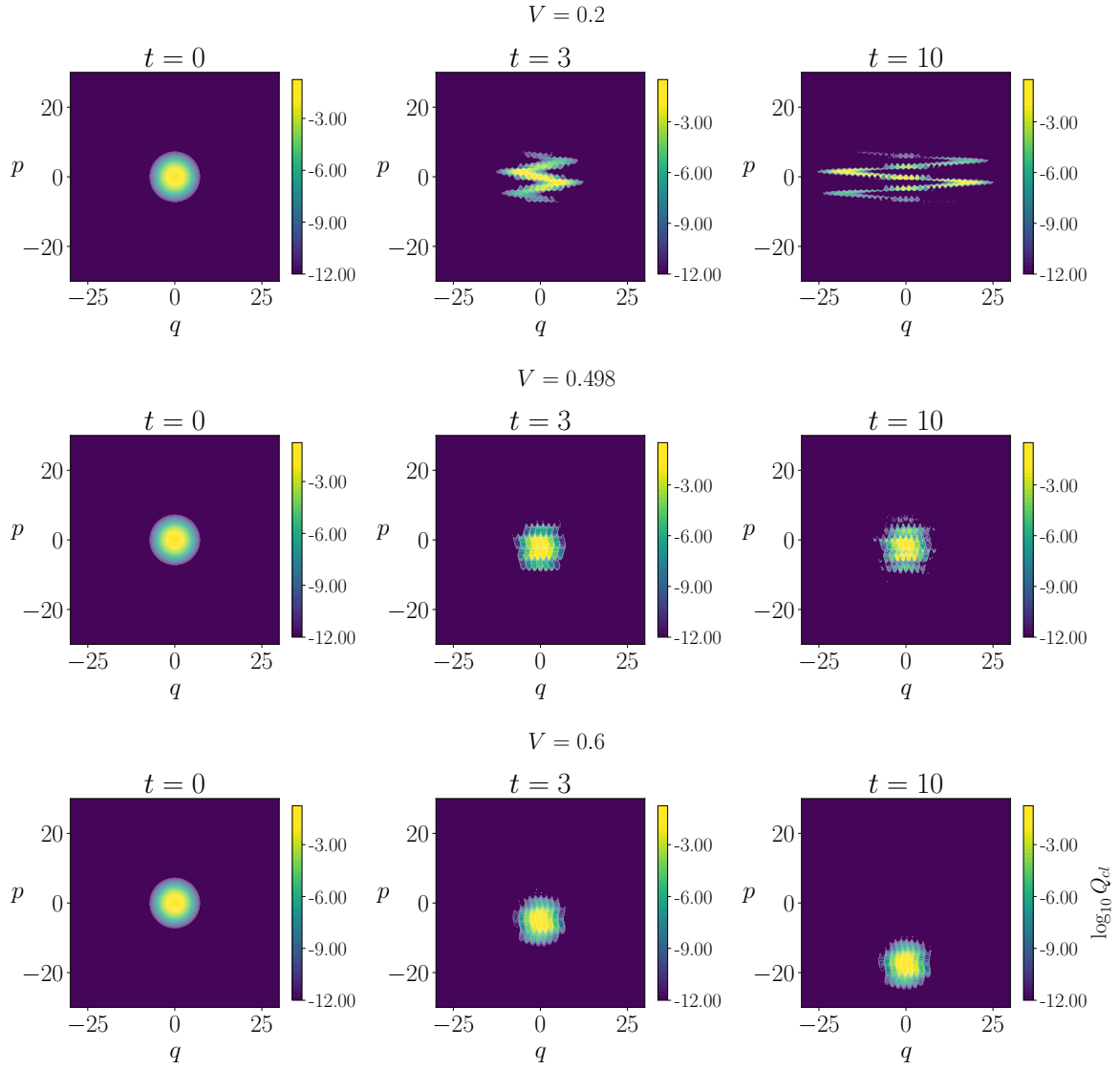


FIG. 8. Semiclassical Husimi distribution at different time instances starting from coherent state  $|0\rangle$  and evolving under the Hamiltonian [Eq. (18)]. Data is for  $V = 0.2, 0.498, 0.6$ . The color code represents the Husimi values.

where the separatrices merge, occurring at  $V_c \sim 0.498$  for  $J = 1$ . All figures shown correspond to the choice  $\beta = (\sqrt{5} - 1)/2$ .

Further comparison of the dynamical properties of the lattice model with the speed of propagation extracted from the time evolution of the Husimi distribution of the corresponding continuous quantum model, as well as from the semiclassical Husimi dynamics, reveals that although both the lattice and continuous quantum models exhibit a transition near  $V \simeq 1$ , the semiclassical description fails to reproduce this behavior (see Fig. 9 lower panel). Instead, the speed of propagation obtained from the semiclassical Husimi evolution drops already near  $V \sim 0.498$ , coinciding with a transition in the classical trajectories. As in Model I, the classical phase transition point systematically underestimates the quantum localization transition.

### 3. Special $\beta$ limit

For a special choice of the irrational parameter, namely  $\beta = \frac{1}{2\pi\sqrt{7}}$  for Model I and  $\beta = \frac{\sqrt{3}}{2\pi}$  for Model II (for our chosen set of parameters), we find that the dynamical behavior and the corresponding phase transition points are qualitatively the same. The results are presented in Fig. 10.

Moreover, to quantify how effectively the classical description mimics the quantum dynamics, we compute the phase-space purity, defined as

$$P(t) = \int |Q_q^{\text{norm}}(q, p, t)|^2 dp dq, \quad (20)$$

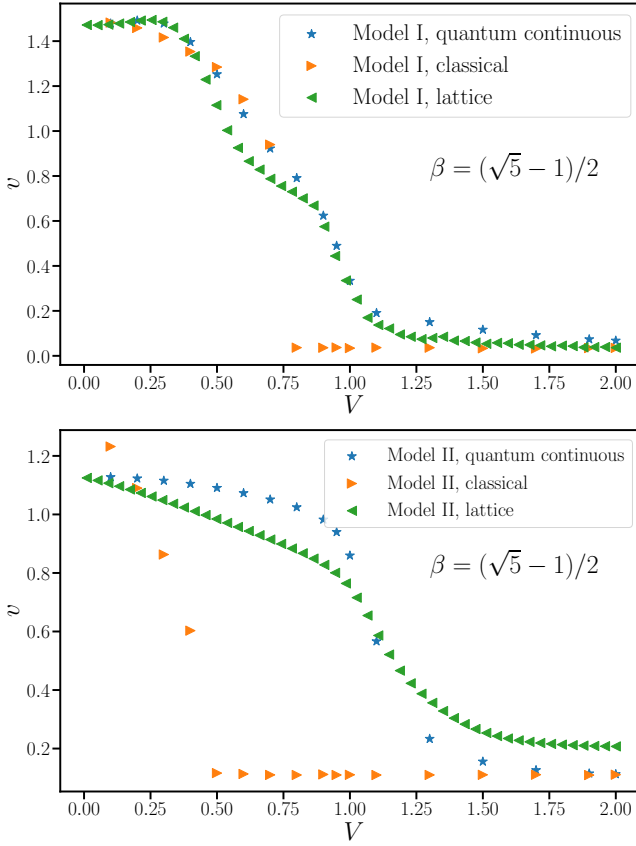


FIG. 9. Upper panel: Comparison of the velocity of the excitation of the lattice Model I Eq. (1) with the excitation velocity extracted from the Husimi distribution of the quantum continuous Model I [Eq. (7)], as well as the velocity extracted from the semiclassical Husimi evolution, data are generated at the time instant  $t = 30$ . We take  $\beta = (\sqrt{5}-1)/2$ . Lower panel: Comparison of the velocity of the excitation of the lattice Model II [Eq. (2)] with the excitation velocity extracted from the Husimi distribution of the quantum continuous Model II [Eq. (8)] and the velocity extracted from the corresponding semiclassical Husimi dynamics, data are generated at the time instant  $t = 10$ . We take  $\beta = (\sqrt{5}-1)/2$ .

where

$$Q_q^{\text{norm}}(q, p, t) = \frac{Q_q(q, p, t)}{\int Q_q(q, p, t) dp dq}.$$

At  $t = 0$ , we initialize the system in a coherent state,

$$Q_q(q, p, 0) = e^{-(q^2+p^2)/2},$$

which yields

$$P(0) = \frac{1}{4\pi}.$$

As time evolves, if  $P(t)$  does not decay rapidly, this indicates that the classical description continues to approximate the quantum dynamics reasonably well within that parameter regime.

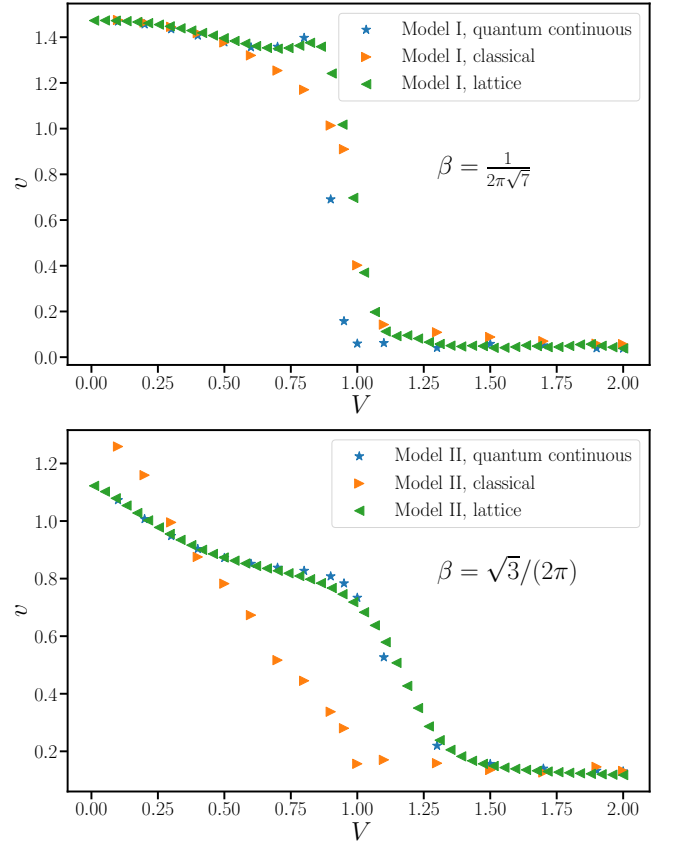


FIG. 10. Upper panel: Comparison of the velocity of the excitation of the lattice Model I [Eq. (1)] with the excitation velocity extracted from the Husimi distribution of the quantum continuous Model I [Eq. (7)], as well as the velocity extracted from the semiclassical Husimi evolution for  $\beta = \frac{1}{2\pi\sqrt{7}}$ , data are generated at the time instant  $t = 30$ . Lower panel: Comparison of the velocity of the excitation of the lattice Model II [Eq. (2)] with the excitation velocity extracted from the Husimi distribution of the quantum continuous Model II [Eq. (8)] and the velocity extracted from the corresponding semiclassical Husimi dynamics for  $\beta = \sqrt{3}/(2\pi)$ , data are generated at the time instant  $t = 10$ .

In the context of quantum–classical correspondence, the relevant timescale is typically the Ehrenfest time,

$$t_E \sim \lambda^{-1}, \quad (21)$$

which determines the duration over which quantum dynamics can be reasonably approximated by classical evolution, with  $\lambda$  denoting the effective Lyapunov exponent (see Eq. (17)). Up to this time, semiclassical descriptions remain valid, whereas beyond it genuine quantum interference effects dominate the dynamics.

For the Hermitian case, it is clear from Eq. (17) (when  $J_R = J_L$ ) that for a given potential strength  $V$ , the regime of large Ehrenfest time corresponds to the limit  $\beta \rightarrow 0$ . In this limit,  $t_E$  becomes extremely large, and presumably the classical–quantum correspondence can be formally well established. However, this limit is of lim-

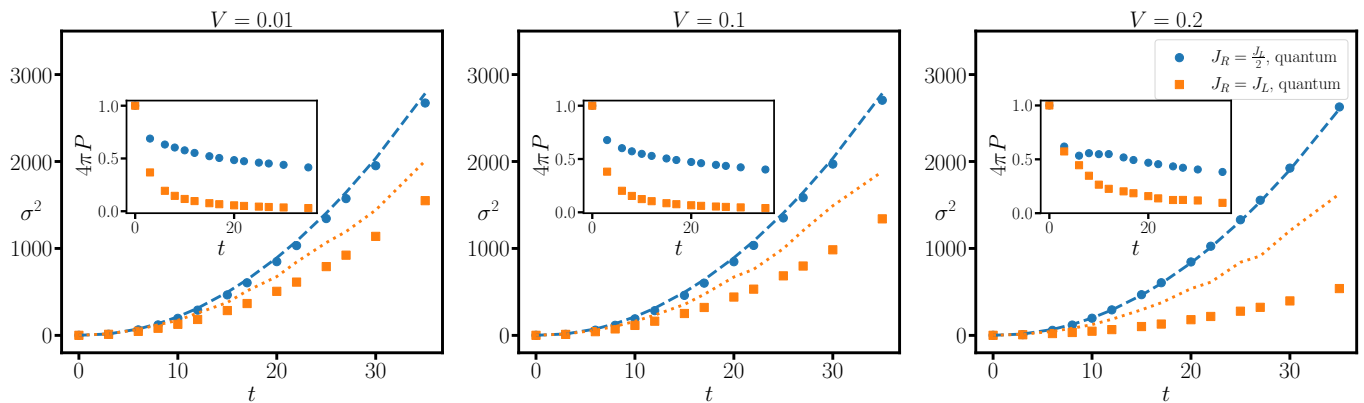


FIG. 11. Main panel: Comparison of  $\sigma^2$  extracted from Quantum and classical Husimi distribution in the limit  $\beta V \rightarrow \frac{\Delta}{4\pi}$ , both for non-Hermitian (Model I with  $J_R = \frac{J_L}{2}$ ) and Hermitian (Model I with  $J_R = J_L$ ). The inset shows the change in the purity with time of the quantum Husimi distribution in the above mentioned limit. Square and circle points represent the data extracted from quantum Husimi with  $J_L = J_R$  and  $J_R = \frac{J_L}{2}$ , respectively, and dotted lines represent the classical data for  $J_L = J_R$ , dashed lines represent the classical data with  $J_R = \frac{J_L}{2}$ .

ited practical relevance. To observe significant quasiperiodic effects in a finite-size lattice, one requires  $\beta$  to be reasonably large. Increasing  $\beta$ , however, reduces the Ehrenfest time and consequently shrinks the temporal window over which classical dynamics faithfully reproduces the quantum evolution. Thus, in the Hermitian case, the classical limit and the physically relevant quasiperiodic regime do not strongly overlap, restricting the practical utility of the semiclassical approximation in dynamics.

The situation changes qualitatively in the non-Hermitian case. There, for model I the regime of large Ehrenfest time corresponds to the condition

$$\beta V \rightarrow \frac{\Delta}{4\pi}, \quad (22)$$

for which  $\lambda \rightarrow 0$  (see Eq. (17)). For fixed and sufficiently small  $V$ , this allows  $\beta$  to take reasonably large values while the system remains in the delocalized phase. Hence, unlike the Hermitian case, the semiclassical regime overlaps with a physically meaningful parameter window.

We demonstrate this explicitly in Fig. 11. In this limit, the purity does not decay rapidly, indicating that quantum interference effects are significantly suppressed. Moreover, the wavepacket width  $\sigma(t)$  can be reproduced with high accuracy using classical evolution based on the Husimi distribution. As shown in the figure, the quantum results (dots) agree remarkably well with the classical Husimi calculations (dashed lines) up to a substantial time scale.

Figure 11 further highlights a crucial contrast: in the same  $\beta$  regime, the Hermitian model fails to reproduce the quantum dynamics even at extremely short times. The classical approximation breaks down almost immediately, implying that the effective Ehrenfest time is very small. This stark difference underscores the qualitative impact of non-Hermiticity.

## VI. CONCLUSION

In the Hermitian Aubry–André (AA) model, the delocalization–localization transition admits a clear semiclassical interpretation: the classical phase-space portrait develops separatrices precisely at the quantum critical point, and the semiclassical Husimi evolution correctly predicts the location of this transition [44]. In this work, we ask whether an analogous correspondence persists in non-Hermitian quasiperiodic lattice models [58, 59], which are also known to exhibit localization–delocalization transitions.

To answer the proposed question, we analyze the Husimi distribution of the quantum state [50, 51], which provides a phase-space representation of the underlying quantum dynamics. Starting from the continuum limit of the non-Hermitian lattice model, we compute the time evolution of the Husimi distribution for an initial coherent state and compare its propagation speed with that obtained directly from the lattice dynamics. The two descriptions show good qualitative agreement. In contrast, the semiclassical Husimi evolution fails to reproduce the quantum localization–delocalization transition point. This failure is consistent with the fact that the trajectory equations governing the semiclassical Husimi dynamics do not predict the correct transition, as demonstrated by our fixed-point analysis, even though these trajectories exhibit a far richer and more intricate structure than their Hermitian counterparts. This highlights a fundamental limitation of semiclassical intuition in non-Hermitian quasiperiodic systems and points to qualitatively new mechanisms governing their localization behavior. Furthermore, unlike the Hermitian Aubry–André case, the transition point of the non-Hermitian lattice model depends explicitly on the incommensurability parameter  $\beta$ , which characterizes the irrational quasiperiodicity of the potential. We identify a special value of

$\beta$  for which the classical and quantum transition points coincide.

This naturally leads to a more fundamental question: are non-Hermitian systems more susceptible to a loss of classicalness than their Hermitian counterparts? Since the validity of semiclassical descriptions relies on the persistence of classical phase-space structures, an enhanced breakdown of classical correspondence could underlie the failure of semiclassical Husimi dynamics observed in non-Hermitian systems. Moreover, the explicit  $\beta$  dependence of the classically predicted localization transition points suggests that the incommensurability parameter plays a much more significant role in non-Hermitian settings, potentially influencing even the quantum localization transition. In Hermitian quasiperiodic models,  $\beta$  is typically taken for granted, as the transition point is independent of its precise value. Our results indicate that this assumption may no longer hold once non-Hermiticity is introduced, and that the role of  $\beta$  warrants careful re-examination in non-Hermitian quantum lattice models.

On the other hand, if one interprets this as a limitation of the semiclassical analysis—namely, its inability to accurately capture the localization transition for arbitrary values of  $\beta$ —our findings nevertheless reveal an important positive aspect. Specifically, we identify a nontrivial and experimentally relevant parameter regime (moderately large  $\beta$ ) in which semiclassical correspondence remains quantitatively reliable within a finite time window in the non-Hermitian system, even though it fails in the corresponding Hermitian counterpart. Such a regime would not have been evident without constructing the explicit classical phase-space correspondence. Our analysis therefore demonstrates that classical Husimi evolution is not merely a qualitative diagnostic tool, but can provide an efficient and quantitatively accurate description of the underlying quantum dynamics over physically relevant timescales.

An intriguing direction is the construction of non-Hermitian models in which the quantum localization transition itself becomes explicitly  $\beta$  dependent. Such a scenario would be especially appealing from an experimental standpoint, since  $\beta$  can be tuned by varying the wavelength ratio of laser potentials in optical lattice realizations. This tunability would offer a direct and controlled way to explore distinct localization transition points within a single experimental platform.

## ACKNOWLEDGMENTS

R.M. acknowledges the DST-Inspire fellowship from the Department of Science and Technology, Government of India, SERB start-up grant (SRG/2021/002152). BPM acknowledges the PDF grant of IOE of Banaras Hindu University, Varanasi for the year 2025-26. The authors gratefully acknowledge S. Y. Ali for valuable discussions during the early stages of this project.

## Appendix A: Trajectory analysis and Husimi dynamics of Hermitian AA model

For the sake of completeness, in this appendix we present the classical trajectory analysis of the Hermitian Aubry–André (AA) model [3]. We find that the transition from the delocalized to the localized phase occurs at  $V_c = J$  in both the quantum and classical versions of the model. The lattice model is given by,

$$H_{AA} = J \sum_i (c_i^\dagger c_{i+1} + c_{i+1}^\dagger c_i) + 2V \sum_i \cos(2\pi\beta i) c_i^\dagger c_i, \quad (\text{A1})$$

here,  $c_i^\dagger, c_i$  are the creation and annihilation operators respectively, and  $V$  is the strength of the quasiperiodic potential.  $\beta$  is an irrational number. In our calculation we take  $\beta = \frac{\sqrt{5}-1}{2}$ . The semiclassical version of the above Hamiltonian, is given by [44, 62],

$$H_{AA}^c = 2J \cos p + 2V \cos(2\pi\beta q). \quad (\text{A2})$$

In our calculation, we take  $J = 1$ . The Hamiltonian equations of motion are,

$$\begin{aligned} \dot{q} &= -\frac{\partial H_{AA}^c}{\partial p} = 2 \sin p \\ \dot{p} &= \frac{\partial H_{AA}^c}{\partial q} = -4\pi\beta V \sin(2\pi\beta q). \end{aligned} \quad (\text{A3})$$

For  $V = 0$ , the potential is absent, and all trajectories are spatially extended, exhibiting ballistic motion with the momentum remaining constant throughout the dynamics. In the opposite limit,  $V \rightarrow \infty$ , the potential term dominates: the kinetic energy becomes negligible, trajectories become trapped (localized) in space by the potential, and are correspondingly delocalized in momentum. In the intermediate regime, a crossover occurs, characterized by the emergence of separatrices that delineate three distinct types of trajectories.

Below, we try to understand this from the fixed point(stationary points) analysis.

Once again, we follow the same strategy as discussed in the main text. First, we identify the fixed points of the dynamical equations as,

$$\begin{aligned} \dot{q} = 0 & \quad \text{gives} \quad p_0 = n\pi, \quad n = 0, \pm 1, \pm 2 \dots \\ \dot{p} = 0 & \quad \text{gives} \quad q_0 = \frac{n\pi}{2\pi\beta}, \quad n = 0, \pm 1, \pm 2 \dots \end{aligned}$$

The eigenvalues of the Jacobian matrix, obtained by linearizing Eq. (A3), are

$$\begin{aligned} (q_0, p_0) = (0, 0) & \quad \text{gives} \quad \lambda = \pm 4Vi(2\pi\beta)^2 \\ (q_0, p_0) = (\pi/(2\pi\beta), \pi) & \quad \text{gives} \quad \lambda = \pm 4Vi(2\pi\beta)^2 \\ (q_0, p_0) = (0, \pi) & \quad \text{gives} \quad \lambda = \pm 4V(2\pi\beta)^2 \\ (q_0, p_0) = (\pi/(2\pi\beta), 0) & \quad \text{gives} \quad \lambda = \pm 4V(2\pi\beta)^2. \end{aligned}$$

Hence, a slight departure from the stable fixed points  $(0, 0)$  and  $(\pi/(2\pi\beta), \pi)$  leads to periodic, bounded orbits.

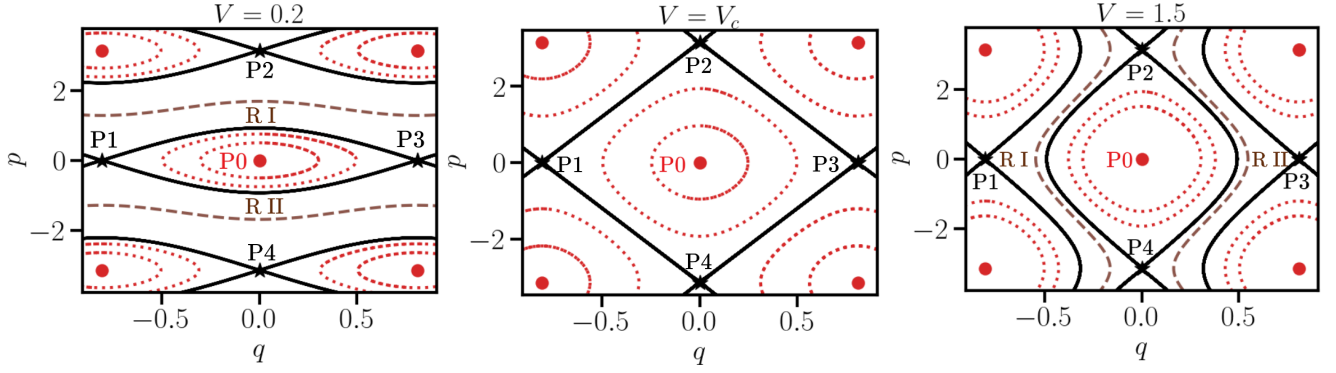


FIG. 12. Trajectory evolution governed by the semiclassical Hamiltonian [Eq. (A2)] at different  $V$  values in the Hermitian case. Trajectory evolution shows a transition near  $V_c = J_L = J_R$ . Data are for  $J_L = 1, J_R = 1$ .

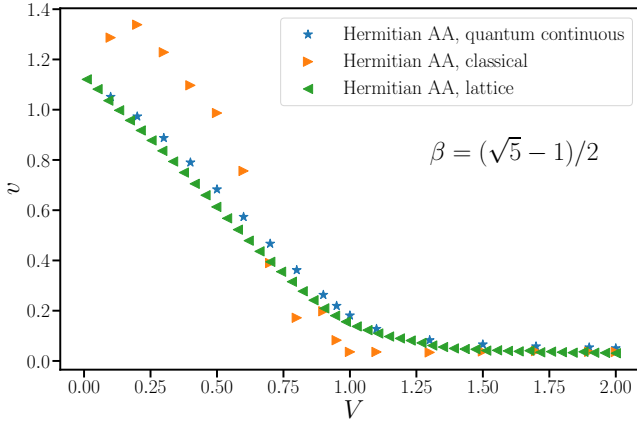


FIG. 13. Comparison of the velocity of the excitation of the Hermitian AA lattice Model with the excitation velocity extracted from the Husimi distribution of the quantum continuous Model, as well as the velocity extracted from the semiclassical Husimi evolution at  $t = 30$ .

In contrast, small deviations from the saddle points  $(0, \pi)$  and  $(\pi/(2\pi\beta), 0)$  give rise to unbounded trajectories, as the corresponding linearized dynamics has one positive real eigenvalue. Since the dynamical equations in Eq. A3 describe a time-independent, energy-conserving Hamilto-

nian system, each trajectory in the phase portrait corresponds to a fixed energy. In order to eliminate the separation between regions I and II for  $V = 0.2$  (see Fig. 12), one must ensure that a single trajectory passes through multiple saddle points, for example P1 and P2, or P1 and P3, and so on. This is possible only when the energies associated with the corresponding saddle points coincide, i.e., when the saddle energies of points such as P1 and P2 merge. This implies,

$$\begin{aligned} H_{AA}^c|_{0,\pi} &= H_{AA}^c|_{\pi/2\pi\beta,0}, \\ -2 + 2V_c &= 2 - 2V_c. \end{aligned}$$

We get  $V_c = 1$ . A similar argument can be drawn from a slope analysis, as discussed in the main text, where the dynamical equations are not Hamiltonian in nature. Note that the critical potential  $V_c$  is independent of  $\beta$ , in contrast to the non-Hermitian case. These results can also be confirmed by performing a numerical trajectory analysis [44, 64], as shown in Fig. 12.

Finally, in Fig. 13, we compare the excitation speed  $v$  as a function of  $V$  for the lattice model, the quantum Husimi calculation in the continuum model, and the classical Husimi distribution, following the same procedure as in the main text for the non-Hermitian case. We find that the phase transition point is correctly captured even by the classical Husimi dynamics, and, unlike the non-Hermitian model, no  $\beta$  dependence is observed.

[1] P. W. Anderson, “Absence of diffusion in certain random lattices,” *Phys. Rev.* **109**, 1492–1505 (1958).  
 [2] Elihu Abrahams, Philip W Anderson, Donald C Licciardello, and Tiruppattur V Ramakrishnan, “Scaling theory of localization: Absence of quantum diffusion in two dimensions,” *Physical Review Letters* **42**, 673 (1979).  
 [3] Serge Aubry and Gilles André, “Analyticity breaking and anderson localization in incommensurate lattices,” *Ann. Israel Phys. Soc* **3**, 18 (1980).  
 [4] Thomas Kohlert, Sebastian Scherg, Xiao Li, Henrik P.

Lüschen, Sankar Das Sarma, Immanuel Bloch, and Monika Aidelsburger, “Observation of many-body localization in a one-dimensional system with a single-particle mobility edge,” *Phys. Rev. Lett.* **122**, 170403 (2019).  
 [5] Henrik P. Lüschen, Sebastian Scherg, Thomas Kohlert, Michael Schreiber, Pranjal Bordia, Xiao Li, S. Das Sarma, and Immanuel Bloch, “Single-particle mobility edge in a one-dimensional quasiperiodic optical lattice,” *Phys. Rev. Lett.* **120**, 160404 (2018).  
 [6] Michael Schreiber, Sean S Hodgman, Pranjal Bordia,

- Henrik P Lüschen, Mark H Fischer, Ronen Vosk, Ehud Altman, Ulrich Schneider, and Immanuel Bloch, “Observation of many-body localization of interacting fermions in a quasirandom optical lattice,” *Science* **349**, 842–845 (2015).
- [7] Fangzhao Alex An, Karmela Padavić, Eric J. Meier, Suraj Hegde, Sriram Ganeshan, J. H. Pixley, Smitha Vishveshwara, and Bryce Gadway, “Interactions and mobility edges: Observing the generalized aubry-andré model,” *Phys. Rev. Lett.* **126**, 040603 (2021).
- [8] Balázs Hetényi, “Scaling of the bulk polarization in extended and localized phases of a quasiperiodic model,” *Phys. Rev. B* **110**, 125124 (2024).
- [9] Balázs Hetényi and István Balogh, “Localization at irrational fillings in the aubry-andré model,” arXiv preprint arXiv:2409.01233 (2024).
- [10] M. Suman, S. Aravinda, and Ranjan Modak, “Probing quantum phase transitions via quantum speed limits,” *Phys. Rev. A* **110**, 012466 (2024).
- [11] Ayan Sahoo, Utkarsh Mishra, and Debraj Rakshit, “Localization-driven quantum sensing,” *Phys. Rev. A* **109**, L030601 (2024).
- [12] Arpita Goswami, “Emergence of single-particle mobility edge (spme) in a ladder network under a modified aubry-andré-harper (aah) kind distortion,” arXiv preprint arXiv:2502.01511 (2025).
- [13] Yucheng Wang, Xu Xia, Yongjian Wang, Zuohuan Zheng, and Xiong-Jun Liu, “Duality between two generalized aubry-andré models with exact mobility edges,” *Phys. Rev. B* **103**, 174205 (2021).
- [14] Andrew J. Daley, “Quantum trajectories and open many-body quantum systems,” *Advances in Physics* **63**, 77–149 (2014), <https://doi.org/10.1080/00018732.2014.933502>.
- [15] EM Graefe, B Longstaff, T Plastow, and R Schubert, “Lindblad dynamics of gaussian states and their superpositions in the semiclassical limit,” *Journal of Physics A: Mathematical and Theoretical* **51**, 365203 (2018).
- [16] F Klauck, Lucas Teuber, Marco Ornigotti, Matthias Heinrich, Stefan Scheel, and Alexander Szameit, “Observation of pt-symmetric quantum interference,” *Nature Photonics* **13**, 883–887 (2019).
- [17] Eva-Maria Graefe, “Pt symmetry dips into two-photon interference,” *Nature Photonics* **13**, 822–823 (2019).
- [18] R Wang, K L Zhang, and Z Song, “Anderson localization induced by complex potential,” *Journal of Physics Communications* **5**, 095011 (2021).
- [19] Stefano Longhi, “Phase transitions in a non-hermitian aubry-andré-harper model,” *Phys. Rev. B* **103**, 054203 (2021).
- [20] Tong Liu, Hao Guo, Yong Pu, and Stefano Longhi, “Generalized aubry-andré self-duality and mobility edges in non-hermitian quasiperiodic lattices,” *Phys. Rev. B* **102**, 024205 (2020).
- [21] Dechi Peng, Shujie Cheng, and Gao Xianlong, “Long-range hopping in a quasiperiodic potential weakens the non-hermitian skin effect,” *Phys. Rev. B* **111**, 094204 (2025).
- [22] Yanxia Liu, Yongjian Wang, Zuohuan Zheng, and Shu Chen, “Exact non-hermitian mobility edges in one-dimensional quasicrystal lattice with exponentially decaying hopping and its dual lattice,” *Phys. Rev. B* **103**, 134208 (2021).
- [23] Ze-Yu Xing, Shu Chen, and Haiping Hu, “Universal spreading dynamics in quasiperiodic non-hermitian systems,” *Phys. Rev. B* **111**, L180203 (2025).
- [24] Qiyun Tang and Yan He, “Mobility edges in non-hermitian models with slowly varying quasiperiodic disorder,” *Phys. Rev. B* **109**, 224204 (2024).
- [25] Ze-Yu Xing, Shu Chen, and Haiping Hu, “Universal spreading dynamics in quasiperiodic non-hermitian systems,” *Phys. Rev. B* **111**, L180203 (2025).
- [26] Soumya Ranjan Padhi, Sanchayan Banerjee, Tanay Nag, and Tapan Mishra, “Anomalous spectrum in a non-hermitian quasiperiodic chain,” *Phys. Rev. B* **112**, 174201 (2025).
- [27] Ashirbad Padhan, Soumya Ranjan Padhi, and Tapan Mishra, “Complete delocalization and reentrant topological transition in a non-hermitian quasiperiodic lattice,” *Physical Review B* **109**, L020203 (2024).
- [28] Li Wang, Zhenbo Wang, and Shu Chen, “Non-hermitian butterfly spectra in a family of quasiperiodic lattices,” *Physical Review B* **110**, L060201 (2024).
- [29] Li Wang, Jiaqi Liu, Zhenbo Wang, and Shu Chen, “Exact complex mobility edges and flagellate-like spectra for non-hermitian quasicrystals with exponential hoppings,” *Physical Review B* **110**, 144205 (2024).
- [30] Ling-Zhi Tang, Guo-Qing Zhang, Ling-Feng Zhang, and Dan-Wei Zhang, “Localization and topological transitions in non-hermitian quasiperiodic lattices,” *Physical Review A* **103**, 033325 (2021).
- [31] Aruna Prasad Acharya and Sanjoy Datta, “Localization transitions in a non-hermitian quasiperiodic lattice,” *Physical Review B* **109**, 024203 (2024).
- [32] Tong Liu and Xu Xia, “Real-complex transition driven by quasiperiodicity: A class of non-pt symmetric models,” *Physical Review B* **105**, 054201 (2022).
- [33] Dipendu Halder and Saurabh Basu, “Controlled probing of localization effects in the non-hermitian aubry-andré model via topoelectrical circuits,” *Phys. Rev. B* **111**, 235447 (2025).
- [34] Quan Lin, Tianyu Li, Lei Xiao, Kunkun Wang, Wei Yi, and Peng Xue, “Topological phase transitions and mobility edges in non-hermitian quasicrystals,” *Phys. Rev. Lett.* **129**, 113601 (2022).
- [35] Wei Gou, Tao Chen, Dizhou Xie, Teng Xiao, Tian-Shu Deng, Bryce Gadway, Wei Yi, and Bo Yan, “Tunable nonreciprocal quantum transport through a dissipative aharonov-bohm ring in ultracold atoms,” *Phys. Rev. Lett.* **124**, 070402 (2020).
- [36] Fangzhao Alex An, Eric J. Meier, and Bryce Gadway, “Engineering a flux-dependent mobility edge in ordered zigzag chains,” *Phys. Rev. X* **8**, 031045 (2018).
- [37] Jiaming Li, Andrew K Harter, Ji Liu, Leonardo de Melo, Yogesh N Joglekar, and Le Luo, “Observation of parity-time symmetry breaking transitions in a dissipative floquet system of ultracold atoms,” *Nature communications* **10**, 855 (2019).
- [38] Liang Feng, Ramy El-Ganainy, and Li Ge, “Non-hermitian photonics based on parity-time symmetry,” *Nature Photonics* **11**, 752–762 (2017).
- [39] Alexander Cerjan, Sheng Huang, Mohan Wang, Kevin P Chen, Yidong Chong, and Mikael C Rechtsman, “Experimental realization of a weyl exceptional ring,” *Nature Photonics* **13**, 623–628 (2019).
- [40] Carl M. Bender and Stefan Boettcher, “Real spectra in non-hermitian hamiltonians having  $\mathcal{PT}$  symmetry,” *Phys. Rev. Lett.* **80**, 5243–5246 (1998).
- [41] Carl M Bender, “Making sense of non-hermitian hamil-

- tonians,” *Reports on Progress in Physics* **70**, 947–1018 (2007).
- [42] Tong Liu and Xu Xia, “Real-complex transition driven by quasiperiodicity: A class of non- $\mathcal{PT}$  symmetric models,” *Phys. Rev. B* **105**, 054201 (2022).
- [43] Sebastian Schiffer, Xia-Ji Liu, Hui Hu, and Jia Wang, “Anderson localization transition in a robust  $\mathcal{PT}$ -symmetric phase of a generalized aubry-andré model,” *Phys. Rev. A* **103**, L011302 (2021).
- [44] Mathias Albert and Patricio Leboeuf, “Localization by bichromatic potentials versus anderson localization,” *Phys. Rev. A* **81**, 013614 (2010).
- [45] Carl M Bender, Stefan Boettcher, and Peter N Meisinger, “symmetric quantum mechanics,” *Journal of Mathematical Physics* **40**, 2201–2229 (1999).
- [46] Eva-Maria Graefe and Roman Schubert, “Wave-packet evolution in non-hermitian quantum systems,” *Phys. Rev. A* **83**, 060101 (2011).
- [47] Eva-Maria Graefe, Michael Höning, and Hans Jürgen Korsch, “Classical limit of non-hermitian quantum dynamics—a generalized canonical structure,” *Journal of Physics A: Mathematical and Theoretical* **43**, 075306 (2010).
- [48] Eva-Maria Graefe, HJ Korsch, and A Rush, “Quasiclassical analysis of bloch oscillations in non-hermitian tight-binding lattices,” *New Journal of Physics* **18**, 075009 (2016).
- [49] Guang Yang, Yong-Kang Li, Yongxu Fu, Zhenduo Wang, and Yi Zhang, “Complex semiclassical theory for non-hermitian quantum systems,” *Phys. Rev. B* **109**, 045110 (2024).
- [50] Katherine Holmes, Wasim Rehman, Simon Malzard, and Eva-Maria Graefe, “Husimi dynamics generated by non-hermitian hamiltonians,” *Phys. Rev. Lett.* **130**, 157202 (2023).
- [51] Joseph Hall, Simon Malzard, and Eva-Maria Graefe, “Semiclassical husimi distributions of schur vectors in non-hermitian quantum systems,” *Phys. Rev. Lett.* **131**, 040402 (2023).
- [52] G. J. Milburn, “Quantum and classical liouville dynamics of the anharmonic oscillator,” *Phys. Rev. A* **33**, 674–685 (1986).
- [53] Alexander Altland and Fritz Haake, “Quantum chaos and effective thermalization,” *Phys. Rev. Lett.* **108**, 073601 (2012).
- [54] Matheus Veronez and Marcus AM de Aguiar, “Phase space flow in the husimi representation,” *Journal of Physics A: Mathematical and Theoretical* **46**, 485304 (2013).
- [55] Matheus Veronez and Marcus AM de Aguiar, “Topological structures in the husimi flow,” *Journal of Physics A: Mathematical and Theoretical* **49**, 065301 (2016).
- [56] G. J. Milburn, “Quantum and classical liouville dynamics of the anharmonic oscillator,” *Phys. Rev. A* **33**, 674–685 (1986).
- [57] Eva-Maria Graefe, Michael Höning, and Hans Jürgen Korsch, “Classical limit of non-hermitian quantum dynamics—a generalized canonical structure,” *Journal of Physics A: Mathematical and Theoretical* **43**, 075306 (2010).
- [58] Stefano Longhi, “Metal-insulator phase transition in a non-hermitian aubry-andré-harper model,” *Phys. Rev. B* **100**, 125157 (2019).
- [59] Stefano Longhi, “Phase transitions in a non-hermitian aubry-andré-harper model,” *Phys. Rev. B* **103**, 054203 (2021).
- [60] Tanmoy Pal, Ranjan Modak, and Bhabani Prasad Mandal, “Parity–time-reversal symmetry-breaking transitions in polymeric systems,” *Phys. Rev. E* **111**, 014421 (2025).
- [61] Archak Purkayastha, Sambuddha Sanyal, Abhishek Dhar, and Manas Kulkarni, “Anomalous transport in the aubry-andré-harper model in isolated and open systems,” *Phys. Rev. B* **97**, 174206 (2018).
- [62] S. Ray, A. Ghosh, and S. Sinha, “Drive-induced delocalization in the aubry-andré model,” *Phys. Rev. E* **97**, 010101 (2018).
- [63] Corentin Morice, Dmitry Chernyavsky, Jasper van Wezel, Jeroen van den Brink, and Ali Moghaddam, “Quantum dynamics in 1d lattice models with synthetic horizons,” *SciPost Physics Core* **5**, 042 (2022).
- [64] Alexandr A Didov, Leonid E Kon’kov, and Denis V Makarov, “Transport through degenerate tori and quantum-to-classical crossover in a driven aubry-andré model,” *The European Physical Journal B* **93**, 13 (2020).